Euro. Jnl of Applied Mathematics (2011), *vol.* 22, *pp.* 455–470. © Cambridge University Press 2011
doi:10.1017/S0956792511000180

Non-linear effects on canonical MEMS models

NICHOLAS D. BRUBAKER and JOHN A. PELESKO

Department of Mathematical Sciences, University of Delaware, Newark, DE 19716, USA
email: brubaker@math.udel.edu, pelesko@math.udel.edu

(*Received 1 November 2010; revised 7 April 2011; accepted 8 April 2011; first published online 6 May 2011*)

In modelling electrostatically actuated micro- and nano-electromechanical systems, researchers have typically relied on a small-aspect ratio to form a leading-order theory. In doing so, small gradient terms are dropped. Although this approximation has been fruitful, its consequences have not been investigated. Here, this approximation is re-examined, and a new theory which includes often neglected small curvature terms is presented. Furthermore, the solution set of the new theory is explored for the unit disk domain and compared to the standard theory. Also, the analytical results are compared to experimental data.

Key words: Prescribed mean curvature; Non-linear eigenvalue problem; Mircoelectromechanical systems; Fold point.

1 Introduction

In the famous lecture of Feynman, 'There's Plenty of Room at the Bottom', he addressed 'the problem of manipulating and controlling things on a small scale' [4]. Furthermore, he issued a challenge to miniaturise technology which, in turn, triggered research in micro- and nano-electromechanical systems (MEMS and NEMS, respectively). While he made many accurate predictions, his most important insight was understanding that 'all things do not simply scale down in proportion'. Specifically, in MEMS and NEMS, forces, such as surface tension and electrostatics dominate macro-scale forces, such as gravity and inertia.

Today, MEMS researchers have capitalised on balancing these forces in a variety of innovative ways, but the ground work goes back to Taylor's study of the coalescence of electrostatically deflected soap films [22]. Although Taylor's motivation was to understand the behaviour of raindrops in electrified clouds, researchers have developed many devices that operate on the same principle: electrostatic actuation. All of these devices, such as micro-mirrors, micro-pumps and micro-switches [18], operate in a similar fashion: a potential difference is applied between mechanical components, which creates a Coulomb force between them. Consequently, the Coulomb force causes the mechanical components to deform.

If one of the mechanical components is an elastic structure, e.g. a soap film, these devices inherit an instability, first observed by Taylor [22], that limits their design space. This instability, named the 'pull-in' instability by Nathanson *et al.* [12], occurs when the potential difference is increased beyond some critical value. Beyond this critical value, the

https://doi.org/10.1017/S0956792511000180 Published online by Cambridge University Press

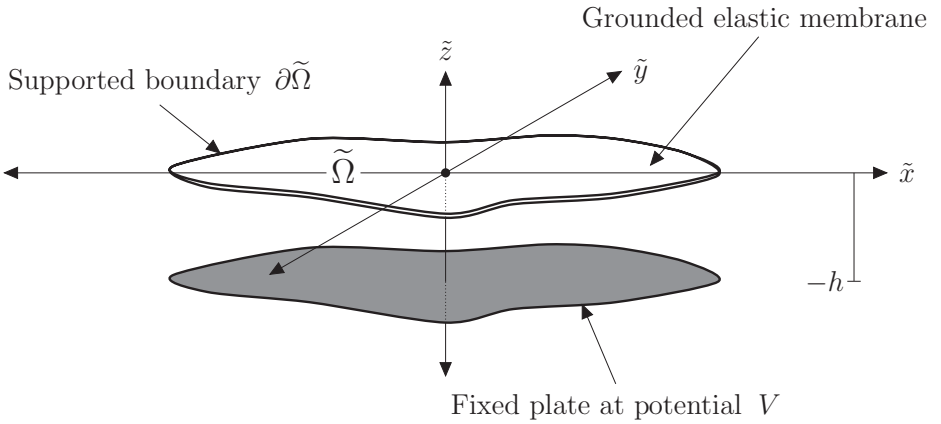


FIGURE 1. Canonical setup.

mechanical components snap together, or, in other words, the separate components have 'pulled-in'. As a result, this critical value is called the 'pull-in' voltage.

As the fields of MEMS and NEMS have rapidly increased, so has the significance of fully understanding electrostatic actuation and its corresponding pull-in instability. To study the various aspects of electrostatically actuated MEMS/NEMS, many authors, following the work of Nathanson *et al.* [12], have used a mass–spring model. While useful, it fails to capture the real geometry and the real elastic effects. To correct this deficiency, Pelesko *et al.* [18] modelled the canonical system, shown in Figure 1, at the core of many MEMS devices. This model is a generalisation of the theory developed by Taylor and Ackerman [1, 22] and, in dimensionless form, can be stated as

$$\Delta u = \frac{\lambda}{(1+u)^2} \quad \text{in} \quad \Omega, \tag{1.1}$$

$$u = 0 \quad \text{on} \quad \partial\Omega. \tag{1.2}$$

Here, $u(x, y)$ describes the shape of the deflected membrane, and the dimensionless parameter λ is defined as

$$\lambda = \frac{\epsilon_0 V^2 L^2}{2h^3 T} \tag{1.3}$$

where ϵ_0 is the permittivity of free space, V is the potential difference between the membrane and the plate, L is the characteristic size of the membrane, h is the distance between the plate and the undeflected membrane and T is the surface tension of the membrane. Note that λ is widely thought of as a 'tuning' parameter because of its proportionality to the square of the potential difference. Therefore, understanding the behaviour of the device is analogous to characterising the solutions for $\lambda > 0$. For this reason, numerous authors have investigated the behaviour of the solutions of equations (1.1) and (1.2). In doing so, the solution set has been shown to have many interesting properties: symmetry breaking in non-simply connected domains [19], multiplicity of solutions [17, 18] and the existence infinitely many solutions for a certain fixed λ [17]. Furthermore, many rigorous results have been derived in [3]. However, no property is

https://doi.org/10.1017/S0956792511000180 Published online by Cambridge University Press

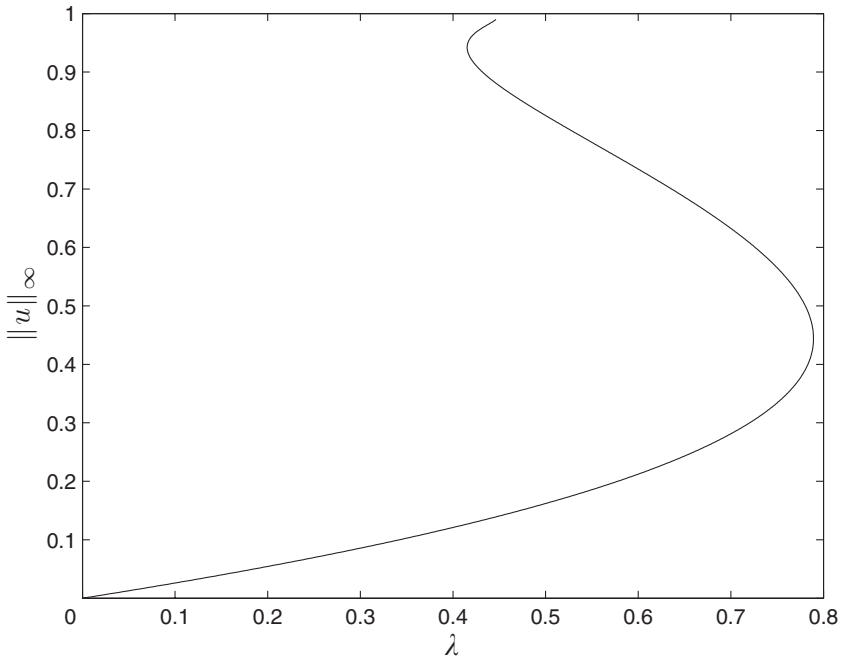


FIGURE 2. Bifurcation diagram for the equations (1.4) and (1.5). The curve folds infinitely many times while $\lambda \to 4/9$ as $\|u\|_\infty \to 1^-$ (cf. [8–11, 14, 16]).

more important than the fact that for an arbitrary domain, no solutions exist for a sufficiently large λ. This is stated in the following theorem:

Theorem 1.1 *Let Ω be a bounded domain in $\mathbb{R}^2$ with smooth boundary $\partial\Omega$. Consider equation (1.1) with Dirichlet boundary condition $u = 0$. Then, there exists a λ^* such that no solution $u \in C^2(\Omega) \cap C(\overline{\Omega})$ exists for any $\lambda > \lambda^*$.*

A proof of this theorem may be found in [18]. The importance of this theorem is that it embodies the ubiquitous 'pull-in' instability of MEMS devices. That is, the non-existence of solutions is generally interpreted as the occurrence of the pull-in. The value of λ^* provides the pull-in voltage of the system V^* and varies for different domains. A specific domain that has been widely studied for equations (1.1) and (1.2) is the unit disk where the problem may be reduced to

$$\frac{\mathrm{d}^2u}{\mathrm{d}r^2} + \frac{1}{r}\frac{\mathrm{d}u}{\mathrm{d}r} = \frac{\lambda}{(1+u)^2} \quad \text{for} \quad 0 < r < 1, \tag{1.4}$$

$$\frac{\mathrm{d}u}{\mathrm{d}r}(0) = 0, \qquad u(1) = 0. \tag{1.5}$$

Note that there are no angular derivatives; this follows from a result of [7], which implies that the solutions are purely radial. Equations (1.4) and (1.5) were studied in [1, 8–11, 14–17]. A key element of equations (1.4) and (1.5) is that the bifurcation diagram of λ versus $\|u\|_\infty = |u(0)|$ contains infinitely many folds with $\lambda \to 4/9$ as $\|u\|_\infty \to 1^-$ (cf. [8–11, 14, 16]). The numerically computed bifurcation diagram is shown in Figure 2 where the

https://doi.org/10.1017/S0956792511000180 Published online by Cambridge University Press

infinite fold point structure starts to reveal itself. Furthermore, many analytical bounds for λ^* have been derived (cf. [6, 8, 18]) and it has been shown numerically that $\lambda^* \approx .7892$ [15].

While much progress has been made in studying the canonical theory and, consequently, given a better understanding of the pull-in instability, the small-aspect ratio used by researchers to simplify their models exhibits a visible weakness: the canonical theory is really a leading-order approximation based on the expansion of a small-aspect ratio. This leads to neglecting the effects of the fringing fields and dropping small gradient terms. The fringing field effects were investigated in [15]. Therefore, the question still remains: how is the solution set altered when the small gradient terms are retained? More specifically, how does the next-order approximation effect λ^*?

In this paper, we develop a corrected model of the canonical system (see Figure 1). We then use this model to investigate the implications on λ^* of retaining the typically neglected terms. We begin the next section by deriving the governing equations. In doing so, we take the deflected component to be an simple, idealised elastic membrane that has negligible bending energy. Moreover, we assume when the membrane's free surface energy is minimised, so too is its surface area – in essence a soap film. Also, in this section, we state and prove a theorem that establishes the existence of a λ^* for our model. In Section 3, we investigate the behaviour of the λ^* for the unit disk domain using perturbation methods. In Section 4, we use our model's predicted λ^* to a formulate next-order correction of the pull-in voltage, V^*. Then, we compare the first-order and second-order predictions of the pull-in voltage V^* to the experimental data in [21]. Finally, in Section 5, we discuss the implications of this work and make suggestions for future work.

2 Model

In this section, we present the governing equations for the shape u of the electrostatically actuated membrane. The system we study is the same system analysed in the canonical theory, i.e. our device consists of a thin elastic membrane suspended above a rigid plate. Moreover, we assume that the elastic membrane is simple and idealised with negligible bending energy, and when its free surface energy minimised, so too is its surface area – e.g. a soap film. The boundary of the membrane and the boundary of the plate are separated by a gap of distance h and fixed on a two-dimensional curve $\partial\widetilde{\Omega}$. To complete the system, a voltage difference is applied between the two components; we take the bottom plate to have potential V and the membrane to be grounded. Recall, this canonical setup is sketched in Figure 1. From this system, we obtain a governing boundary value problem for u by minimising an energy functional.

The main energies present in the system are electrostatic and elastic. Denoting the electrostatic potential by $\tilde{\psi}(\tilde{x}, \tilde{y}, \tilde{z})$, we have that $\tilde{\psi}$ satisfies

$$\tilde{\Delta}\tilde{\psi} = 0, \quad \tilde{\psi}\,(\tilde{x}, \tilde{y}, \tilde{u}(\tilde{x}, \tilde{y})) = 0, \quad \tilde{\psi}\,(\tilde{x}, \tilde{y}, -h) = V, \tag{2.1}$$

where $\tilde{\Delta}$ is the Laplacian with respect to the dimensional variables. Next, we introduce

https://doi.org/10.1017/S0956792511000180 Published online by Cambridge University Press

the dimensionless variables

$$x = \frac{\tilde{x}}{L}, \quad y = \frac{\tilde{y}}{L}, \quad u = \frac{\tilde{u}}{h}, \quad \psi = \frac{\tilde{\psi}}{V}, \quad z = \frac{\tilde{z}}{h}, \tag{2.2}$$

where L is a characteristic distance across the membrane. Substituting these into equation (2.1), we obtain

$$\epsilon^2 \left(\frac{\partial^2 \psi}{\partial x^2} + \frac{\partial^2 \psi}{\partial y^2} \right) + \frac{\partial^2 \psi}{\partial z^2} = 0, \tag{2.3}$$

$$\psi\,(x, y, u(x, y)) = 0, \quad \psi\,(x, y, -1) = 1. \tag{2.4}$$

Here, $\epsilon = h/L$ and, because of the small-aspect ratio of a typical MEMS device, $\epsilon^2 \ll 1$. Thus, solving equations (2.3) and (2.4) after taking $\epsilon \to 0$ gives the dimensionless electrostatic potential

$$\psi(x, y, z) = \frac{u(x, y) - z}{1 + u(x, y)}. \tag{2.5}$$

The electrostatic energy $\mathscr{E}_1$ is given by

$$\mathscr{E}_1 = -\frac{\epsilon_0}{2} \iiint_{\tilde{V}} |\tilde{\nabla}\tilde{\psi}|^2 \, \mathrm{d}\tilde{x}\, \mathrm{d}\tilde{y}\, \mathrm{d}\tilde{z}, \tag{2.6}$$

where the integral is taken over the region between the membrane and the plate, and ϵ_0 is the permittivity of free space. By Green's first identity and equations (2.2) and (2.5), the electrostatic field energy of the system becomes

$$\mathscr{E}_1 = -\frac{\epsilon_0 V^2 L^2}{2h} \iint_{\Omega} \frac{1}{1 + u(x, y)} \, \mathrm{d}x\, \mathrm{d}y. \tag{2.7}$$

Also, the integral is taken over the dimensionless area Ω of the initial membrane.

Given that the free surface energy $\mathscr{E}_2$ is the surface tension T times the change in surface area of the elastic membrane [5], we have

$$\mathscr{E}_2 = TL^2 \iint_{\Omega} \left(\sqrt{1 + \epsilon^2 |\nabla u|^2} - 1 \right) \mathrm{d}x\, \mathrm{d}y. \tag{2.8}$$

Thus, the energy functional of the system is given by

$$\mathscr{E}[u] = \iint_{\Omega} \left(TL^2 \sqrt{1 + \epsilon^2 |\nabla u|^2} - TL^2 - \frac{\epsilon_0 V^2 L^2}{2h} \frac{1}{1 + u} \right) \mathrm{d}x\, \mathrm{d}y. \tag{2.9}$$

Finally, we minimise the total energy $\mathscr{E}$ by taking the first variational derivative and obtain the following partial differential equation for the shape of the membrane $u(x, y)$:

$$\nabla \cdot \frac{\nabla u}{\sqrt{1 + \epsilon^2 |\nabla u|^2}} = \frac{\lambda}{(1 + u)^2}. \tag{2.10}$$

Here, λ is the same dimensionless parameter as defined in the standard canonical theory, equation (1.3), and characterises the relative strengths of the electrostatic and elastic

https://doi.org/10.1017/S0956792511000180 Published online by Cambridge University Press

forces. Recall that we may think of λ as a 'tuning' parameter that depends on the voltage. To complete the general model, we require that the boundary of the membrane stay fixed

$$u|_{\partial\Omega} = 0, \tag{2.11}$$

where $\partial\Omega$ is the dimensionless boundary of the undeflected membrane. Therefore, equations (2.10) and (2.11) form our general curvature-corrected model for the shape of the deflected membrane. First, note that the right-hand side of equation (2.10) is the same as equation (1.1) and captures the Coulomb force. Second, the left-hand side of equation (2.10) is a scaled version of the mean curvature operator. In comparison, the standard canonical theory makes an approximation to this operator by taking its linearisation as in equation (1.1). The effects of not linearising this operator are unknown. Specifically, does a λ^* exist for equations (2.10) and (2.11)? And, if so, how does it vary with ϵ?

As expected, a λ^* does exist for equations (2.10) and (2.11). First, we prove the following lemma.

Lemma 2.1 *If $u \in C^2(\Omega) \cap C(\overline{\Omega})$ is a solution of equation* (2.10) *with $u = 0$ on $\partial\Omega$, then $u < 0$ in Ω.*

Proof Because $u \in C^2(\Omega) \cap C(\overline{\Omega})$ is a solution of equations (2.10) and (2.11), we have that u satisfies

$$\mathscr{F}(x, u, u_x, u_y, u_{xx}, u_{xy}, u_{yy}) = \frac{\lambda}{(1+u)^2}(1 + \epsilon^2|\nabla u|^2)^{3/2} \tag{2.12}$$

in Ω with $u = 0$ on $\partial\Omega$, where

$$\mathscr{F}(x, u, u_x, u_y, u_{xx}, u_{xy}, u_{yy}) := \Delta u + \epsilon^2\left(u_y^2 u_{xx} + u_x^2 u_{yy} - 2u_x u_y u_{xy}\right). \tag{2.13}$$

Since the right-hand side of (2.12) is greater than or equal to zero

$$\mathscr{F}(x, u, u_x, u_y, u_{xx}, u_{xy}, u_{yy}) \geqslant 0 = \mathscr{F}(x, v, v_x, v_y, v_{xx}, v_{xy}, v_{yy}), \tag{2.14}$$

where $v \equiv 0$ in $\overline{\Omega}$. Hence, since $u = v = 0$ on $\partial\Omega$, we have, by Theorem 2.1.4 in [20], $u < v \equiv 0$ in Ω. □

With this result in hand, we can prove the following theorem.

Theorem 2.2 *Let Ω be a bounded domain in $\mathbb{R}^2$ with piecewise smooth boundary $\partial\Omega$. If $u \in C^2(\Omega) \cap C(\overline{\Omega})$ is a solution of equation (2.10) with Dirichlet boundary conditions and $\epsilon > 0$, then*

$$\lambda < \frac{1}{\epsilon}\frac{|\partial\Omega|}{|\Omega|}, \tag{2.15}$$

where $|\partial\Omega|$ is the length of $\partial\Omega$ and $|\Omega|$ is the area of Ω.

https://doi.org/10.1017/S0956792511000180 Published online by Cambridge University Press

Proof Integrating over the domain Ω, we obtain

$$\iint_{\Omega} \nabla \cdot \frac{\nabla u}{\sqrt{1+\epsilon^2 |\nabla u|^2}} \, \mathrm{d}x \, \mathrm{d}y = \iint_{\Omega} \frac{\lambda}{(1+u)^2} \, \mathrm{d}x \, \mathrm{d}y. \tag{2.16}$$

By scaling and Lemma 2.1, we know $-1 < u < 0$ that implies $0 < (1+u)^2 < 1$ in Ω. Consequently,

$$\iint_{\Omega} \frac{\lambda}{(1+u)^2} \, \mathrm{d}x \, \mathrm{d}y > \iint_{\Omega} \lambda \, \mathrm{d}x \, \mathrm{d}y = \lambda \, |\Omega| \, . \tag{2.17}$$

Using the divergence theorem, inequality (2.17) becomes

$$\int_{\partial\Omega} \frac{\nabla u \cdot \mathbf{n}}{\sqrt{1+\epsilon^2 |\nabla u|^2}} \, \mathrm{d}s > \lambda \, |\Omega| \, . \tag{2.18}$$

Hence, since the right-hand side of the previous equation is positive

$$\epsilon \lambda \, |\Omega| < \epsilon \left| \int_{\partial\Omega} \frac{\nabla u \cdot \mathbf{n}}{\sqrt{1+\epsilon^2 |\nabla u|^2}} \, \mathrm{d}s \right| \leqslant \int_{\partial\Omega} \frac{\epsilon |\nabla u \cdot \mathbf{n}|}{\sqrt{1+\epsilon^2 |\nabla u|^2}} \, \mathrm{d}s, \tag{2.19}$$

and from Cauchy–Schwarz inequality, $|\mathbf{a} \cdot \mathbf{b}| \leqslant |\mathbf{a}||\mathbf{b}|$, we deduce

$$\epsilon \lambda \, |\Omega| < \int_{\partial\Omega} \frac{\epsilon \, |\nabla u| \, |\mathbf{n}|}{\sqrt{1+\epsilon^2 |\nabla u|^2}} \, \mathrm{d}s. \tag{2.20}$$

Now, $\mathbf{n}$ is an exterior unit normal, $|\mathbf{n}| = 1$, and

$$\frac{\epsilon \, |\nabla u|}{\sqrt{1+\epsilon^2 |\nabla u|^2}} < 1. \tag{2.21}$$

Therefore, equation (2.20) becomes

$$\epsilon \lambda \, |\Omega| < \int_{\partial\Omega} \mathrm{d}s = |\partial\Omega| \, , \tag{2.22}$$

and we have our result

$$\lambda < \frac{1}{\epsilon} \frac{|\partial\Omega|}{|\Omega|}. \tag{2.23}$$

□

From this theorem, we have the following corollary.

Corollary 2.2.1 *There exists a λ^* such that no solution $u \in C^2(\Omega) \cap C(\overline{\Omega})$ of equations (2.10) and (2.11) exists for any $\lambda > \lambda^*$.*

Proof This follows from the contrapositive of Theorem 2.2. □

https://doi.org/10.1017/S0956792511000180 Published online by Cambridge University Press

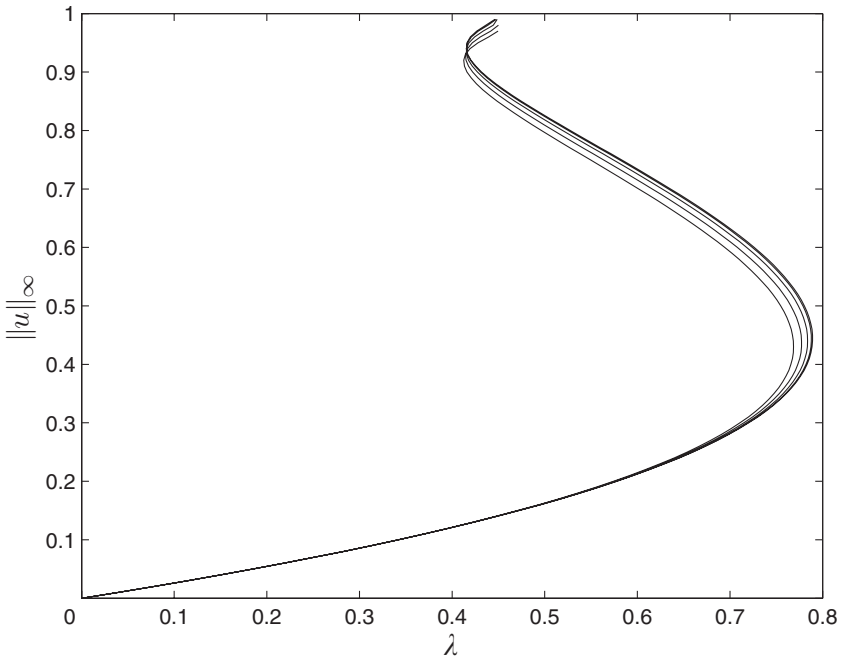


FIGURE 3. Bifurcation diagrams of the disk model (2.24)–(2.25) for several values of ϵ. From right to left (at the largest bump), the solution curves correspond to $\epsilon = 0.1, 0.2, 0.3, 0.4$.

Corollary 2.2.1 implies that like the standard theory, there exists a pull-in voltage V^* for equations (2.10) and (2.11). To see how the pull-in voltage changes, we need to investigate how λ^* varies with respect to ϵ.

From here, we proceed in the case where the domain Ω is the unit disk in $\mathbb{R}^2$. This not only provides us with a simplification but gives us access to experimental data for comparison [21]. Thus, using a change of variables and assuming radial symmetry, equation (2.10) can be reduced to the following ODE for $u(r)$:

$$\frac{1}{r}\left(\frac{ru'}{\sqrt{1+\epsilon^2(u')^2}}\right)' = \frac{\lambda}{(1+u)^2} \qquad \text{for} \quad 0 < r < 1, \tag{2.24}$$

where λ is the same as in equation (2.10) and $'$ denotes $\mathrm{d}/\mathrm{d}r$. The new boundary conditions become

$$u'(0) = 0, \quad u(1) = 0. \tag{2.25}$$

Moreover, by Theorem 2.2, for a solution equations (2.24) and (2.25) to exist, we need $\lambda < 2/\epsilon$. To compute the bifurcation diagram, we use a shooting method. That is, we impose the initial conditions

$$u'(0) = 0, \quad u(0) = \alpha \tag{2.26}$$

and find the λ such that $u(1) = 0$. Here, $\alpha \in (-1, 0)$. In doing this, we obtain the bifurcation diagrams, Figure 3, for various ϵ. Unfortunately as $u(0) \to -1^+$ numerical difficulties arise. Therefore, we parameterise the membrane by arc length s. That is, we let the membrane

https://doi.org/10.1017/S0956792511000180 Published online by Cambridge University Press

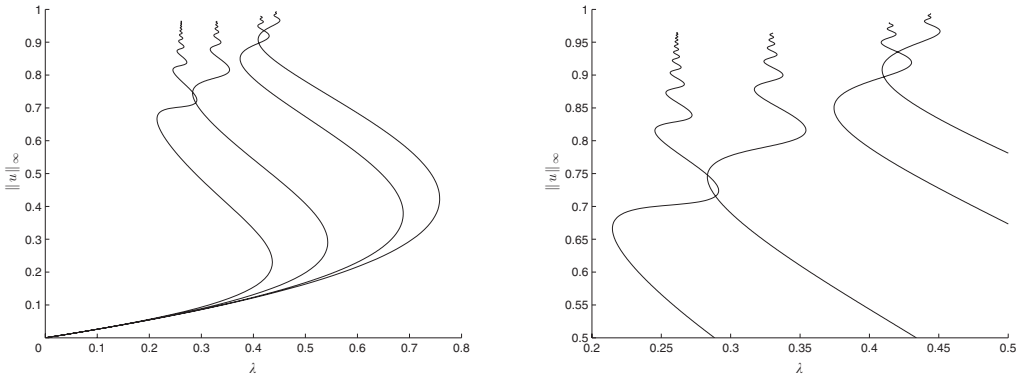


FIGURE 4. (a) Bifurcation diagrams of the disk model (2.27)–(2.28) for several values of ϵ. From right to left (at the largest bump), the curves correspond to $\epsilon = 0.5, 1, 2, 3$. (b) A magnified portion of (a).

be defined in cylindrical coordinates, $r(s)$ and $z(s)$, and rewrite equations (2.24) and (2.25) as

$$r'z'' - z'r'' + \frac{z'}{r} = \frac{\lambda}{(1+z)^2} \qquad \text{for} \quad 0 < s < S, \tag{2.27}$$

$$z(S) = 0, \qquad z'(0) = 0, \qquad r(0) = 0, \qquad r'(0) = \sqrt{1 - \epsilon^2 z'(0)^2} = 1. \tag{2.28}$$

where S is the arc length of the membrane. Then, multiplying equation (2.27) by r' and then separately by z', and using $(r')^2 + \epsilon^2 (z')^2 = 1$, we obtain the following system of second-order ordinary differential equations:

$$z'' = \frac{\lambda r'}{(1+z)^2} - \frac{r'z'}{r}, \qquad r'' = -\frac{\epsilon^2 \lambda z'}{(1+z)^2} + \frac{\epsilon^2 (z')^2}{r} \qquad \text{for} \quad 0 < s < S. \tag{2.29}$$

Also, the initial conditions, equation (2.26), become

$$z(0) = \alpha, \qquad z'(0) = 0, \qquad r(0) = 0, \qquad r'(0) = \sqrt{1 - \epsilon^2 z'(0)^2} = 1. \tag{2.30}$$

Using a shooting procedure as before, we can find solutions of equations (2.27) and (2.28) and compute the bifurcation diagram with higher precision as $\|u\|_\infty = |\alpha| \to -1^+$. The results of this are shown in Figure 4. As in the standard theory, the bifurcation curves appear to have infinitely many folds as $\|u\|_\infty = |\alpha| \to -1^+$; however, the solutions of equations (2.27) and (2.28) are not necessarily solutions to equations (2.24) and (2.25). Specifically, for $|u(0)|$ sufficiently close to 1, the solutions of equations (2.27) and (2.28) cannot be represented as functions of r, as shown in Figure 5, and, consequently, solutions seem to 'disappear'. This seems to be similar to the behaviour observed in some one-dimensional prescribed mean curvature equations (cf. [2, 13]). Currently, the authors are looking at the one-dimensional solution set of equations (2.10) and (2.11) to see if it sheds any light on this two-dimensional radially symmetric case. Regardless, when ϵ is

https://doi.org/10.1017/S0956792511000180 Published online by Cambridge University Press

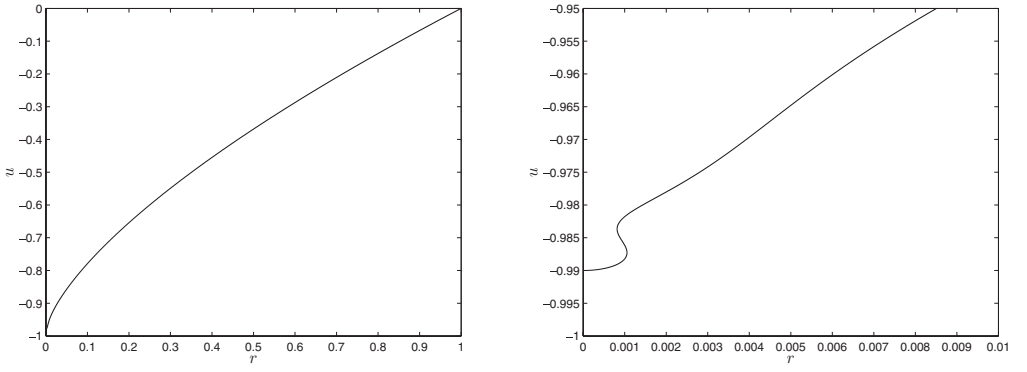


FIGURE 5. (a) Solution of equation (2.27) and (2.28) for $\epsilon = 0.5$, $\lambda = 0.4425\ldots$ and $u(0) = -0.99$. (b) A magnified portion of (a). This shows that the membrane cannot be represented as a function of r.

varied, the locations of the folds change. Therefore, to study how λ^* changes, we need to investigate how the folds move with respect to ϵ.

3 Perturbation analysis

In this section, we investigate the behaviour of the first two folds as they vary with ϵ. We follow the procedure of [10]. That is, we consider the bifurcation diagram of the perturbed problem, Figure 3, as $(\lambda(\alpha), \alpha)$, where $\alpha = u(0)$. Here, we denote the first two fold points by $(\lambda_j^*, \alpha_j^*)$, $\lambda_j^* = \lambda(\alpha_j^*)$, for $j = 1, 2$, respectively. Indicated by the bifurcation diagram, the fold point location $(\lambda_j^*, \alpha_j^*)$ of the jth fold is established by the condition

$$\frac{\mathrm{d}\lambda}{\mathrm{d}\alpha}(\alpha_j^*) = 0. \tag{3.1}$$

Note that λ changes with respect to ϵ. For that reason, we assume

$$\lambda(\alpha) = \lambda_0(\alpha) + \epsilon^2\lambda_1(\alpha) + \mathcal{O}(\epsilon^4). \tag{3.2}$$

Thus, to determine the location of the fold point, we assume $\alpha_j^* = \alpha_{j,0} + \epsilon^2\alpha_{j,1} + \ldots$ and expand and simplify $\lambda_j^* = \lambda(\alpha_j^*)$ using equations (3.1) and (3.2). In doing this, we find that the two-term expansion for each fold point, $(\lambda_j^*, \alpha_j^*)$, when $0 < \epsilon \ll 1$ is given by

$$\lambda_j^* = \lambda_0(\alpha_{j,0}) + \epsilon^2\lambda_1(\alpha_{j,0}) + \mathcal{O}(\epsilon^4). \tag{3.3}$$

Hence, we need to compute $\lambda_0(\alpha_{j,0})$ and $\lambda_1(\alpha_{j,0})$. It should be remarked that $(\lambda_0(\alpha_{j,0}), \alpha_{j,0})$ is the jth fold point of the unperturbed problem.

Together with equation (3.2), we assume

$$u(r) = u_0(r) + \epsilon^2 u_1(r) + \mathcal{O}(\epsilon^4). \tag{3.4}$$

https://doi.org/10.1017/S0956792511000180 Published online by Cambridge University Press

Therefore, at $\mathcal{O}(1)$, we obtain

$$u_0'' + \frac{1}{r}u_0' = \frac{\lambda_0}{(1+u_0)^2} \tag{3.5}$$

with boundary conditions

$$u_0'(0) = u_0(1) = 0. \tag{3.6}$$

This $\mathcal{O}(1)$ problem is the model for the standard theory corresponding to the disk-shaped domain. As mentioned before, it is well known to have infinitely many folds with the first one at $(\lambda_0(\alpha_{1,0}), \alpha_{1,0}) \approx (0.7892, -0.4429)$. The second fold is at $(\lambda_0(\alpha_{2,0}), \alpha_{2,0}) \approx (0.4151, -0.9422)$. Using these values, we can find the leading-order solution at the first two fold points: solutions $u_0^*(r;\alpha_{1,0})$ and $u_0^*(r;\alpha_{2,0})$, respectively.

At $\mathcal{O}(\epsilon^2)$, we have

$$\mathcal{L}u_1 = \frac{\lambda_1 + \frac{3}{2}\lambda_0(u_0')^2}{(1+u_0)^2} - \frac{1}{r}(u_0')^3 \tag{3.7}$$

with boundary conditions

$$u_1'(0) = u_1(1) = 0, \tag{3.8}$$

where

$$\mathcal{L}\varphi := \varphi'' + \frac{1}{r}\varphi' + \frac{2\lambda_0}{(1+u_0)^3}\varphi. \tag{3.9}$$

At the fold location $\alpha = \alpha_{j,0}$, the $\mathcal{O}(\epsilon^2)$ equation becomes

$$\mathcal{L}u_1 = \frac{\frac{3}{2}\lambda_0(\alpha_{j,0})(u_0')^2 + \lambda_1(\alpha_{j,0})}{(1+u_0)^2} - \frac{1}{r}(u_0')^3 \tag{3.10}$$

with the same boundary conditions as before. For our asymptotic expansion to work, we need a unique solution at this order. To this end, we call on the Fredholm Alternative. Accordingly, we need all non-trivial solutions to the homogeneous problem, $\mathcal{L}u_1 = 0$, to be orthogonal with respect to the L^2 inner product to

$$\frac{\frac{3}{2}\lambda_0(\alpha_{j,0})(u_0')^2 + \lambda_1(\alpha_{j,0})}{(1+u_0)^2} - \frac{1}{r}(u_0')^3. \tag{3.11}$$

By differentiating equation (3.5) with respect to α, we obtain

$$\left(\frac{\partial u_0}{\partial \alpha}\right)'' + \frac{1}{r}\left(\frac{\partial u_0}{\partial \alpha}\right)' = -\frac{2\lambda_0}{(1+u_0)^3}\left(\frac{\partial u_0}{\partial \alpha}\right) + \frac{1}{(1+u_0)^2}\frac{\mathrm{d}\lambda_0}{\mathrm{d}\alpha}, \tag{3.12}$$

where $'$ denotes the derivative with respect to r. Namely, since $\mathrm{d}\lambda_0/\mathrm{d}\alpha = 0$ at $\alpha = \alpha_{j,0}$,

$$\left(\frac{\mathrm{d}u_0}{\mathrm{d}\alpha}\right)'' + \frac{1}{r}\left(\frac{\partial u_0}{\partial \alpha}\right)' + \frac{2\lambda_0(\alpha_{j,0})}{(1+u_0)^3}\left(\frac{\partial u_0}{\partial \alpha}\right) = 0. \tag{3.13}$$

In other words, at each unperturbed fold point $\alpha = \alpha_{j,0}$, $\frac{\partial u_0}{\partial \alpha}(r;\alpha_{j,0})$ is a non-trivial solution to the homogeneous $\mathcal{O}(\epsilon^2)$ problem. Thus, to have a unique solution, we utilise the

https://doi.org/10.1017/S0956792511000180 Published online by Cambridge University Press

Fredholm solvability condition to solve for $\lambda_1(\alpha_{j,0})$. In doing this, we find

$$\lambda_1(\alpha_{j,0}) = \frac{\int_0^1 \frac{\partial u_0}{\partial \alpha}\left(\frac{1}{r}(u_0{}')^3 - \frac{\frac{3}{2}\lambda_0(\alpha_{j,0})(u_0{}')^2}{(1+u_0)^2}\right) r\,\mathrm{d}r}{\int_0^1 \frac{\partial u_0}{\partial \alpha}\frac{1}{(1+u_0)^2} r\,\mathrm{d}r}. \tag{3.14}$$

The results of this asymptotic analysis are encapsulated in the following theorem.

Principle Result 3.1 *If $(\lambda_0(\alpha_{j,0}), \alpha_{j,0})$ is the location of the jth fold point of equations (3.5) and (3.6), then the two-term expansion for the jth perturbed fold point of equations (2.24) and (2.25) is given by*

$$\lambda_j^* = \lambda_0(\alpha_{j,0}) + \epsilon^2\lambda_1(\alpha_{j,0}) + \mathcal{O}(\epsilon^4), \tag{3.15}$$

where $\lambda_1(\alpha_{j,0})$ is defined by equation (3.14).

To make use of this result recall that the first and second unperturbed fold points were determined to be

$$(\lambda_0(\alpha_{1,0}), \alpha_{1,0}) \approx (0.7892, -0.4429) \tag{3.16}$$

and

$$(\lambda_0(\alpha_{2,0}), \alpha_{2,0}) \approx (0.4153, -0.9422), \tag{3.17}$$

respectively. Then, $\lambda_1(\alpha_{1,0})$ and $\lambda_1\left(\alpha_{2,0}\right)$ are calculated by equation (3.14). As a result, equation (3.15) gives the explicit two-term expansions for the first fold and second fold that are valid for $\epsilon \ll 1$. They are

$$\lambda_1^* = 0.7892 - 0.1360\epsilon^2 + \ldots \tag{3.18}$$

and

$$\lambda_2^* = 0.4153 + 0.0060\epsilon^2 + \ldots, \tag{3.19}$$

respectively. Now, using $\lambda_0(\alpha_{j,0})$ and $\lambda_1(\alpha_{j,0})$, we can solve the $\mathcal{O}(1)$ and $\mathcal{O}(\epsilon^2)$ to obtain $u_{j,0}^*(x)$ and $u_{j,1}^*(x)$ for the leading-order solution at the fold point. Hence, from equation (3.4), we have a two-term asymptotic approximation

$$u(r;\lambda_j^*) = u_{j,0}^*(r) + \epsilon^2 u_{j,1}^*(r) + \ldots \tag{3.20}$$

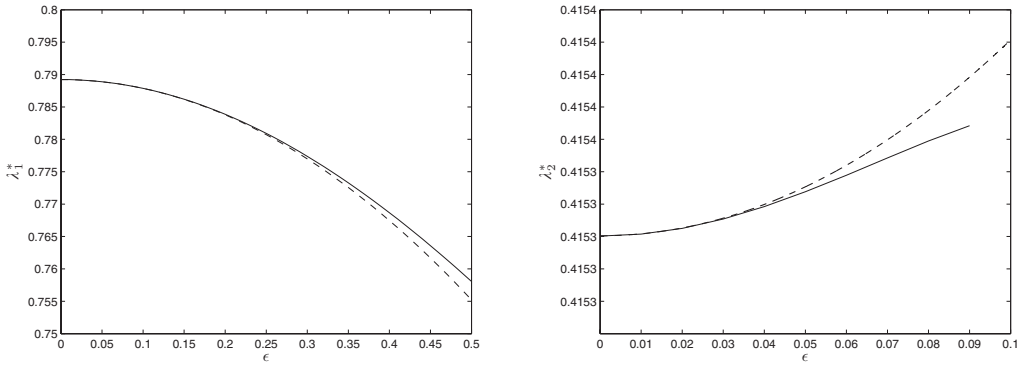
for the leading-order solution at the fold point.

In Figure 6, a comparison of the two-term asymptotic results for λ_1^* and λ_2^* versus ϵ and the full numerical result is provided. The two-term asymptotic approximation is seen to provide a very good approximation of λ^*.

4 Experimental

In this section, we compare our asymptotic results from Section 3 to the experimental results for the pull-in voltage of Siddique *et al.* [21]. Recall from equation (3.3) that we

https://doi.org/10.1017/S0956792511000180 Published online by Cambridge University Press



(a) (b)

FIGURE 6. (a) Comparison of the numerically computed first fold point λ_1^* (line) versus ϵ with the two-term asymptotic result from equation (3.18) (dashed line). (b) Comparison of the numerically computed second fold point λ_2^* (line) versus ϵ with the two-term asymptotic result from equation (3.18) (dashed line).

expanded the first fold point λ_1^* as

$$\lambda_1^* = \lambda_0(\alpha_{1,0}) + \epsilon^2 \lambda_1(\alpha_{1,0}) + \mathcal{O}(\epsilon^4). \tag{4.1}$$

Furthermore, we know that the first fold corresponds to the pull-in voltage V^*; hence,

$$\lambda_1^* = \frac{\epsilon_0 (V^*)^2 L^2}{2h^3 T}. \tag{4.2}$$

Solving for V^* after equating equations (4.1) and (4.2) and using the definition of ϵ, we obtain the two-term asymptotic expansion of the pull-in voltage

$$V^* = \sqrt{\lambda_0(\alpha_{1,0})}\sqrt{\frac{2T}{\epsilon_0 L^2}} h^{3/2} + \frac{\lambda_1(\alpha_{1,0})}{2\sqrt{\lambda_0(\alpha_{1,0})}}\sqrt{\frac{2T}{\epsilon_0 L^6}} h^{7/2}, \tag{4.3}$$

where, as before, $\lambda_0(\alpha_{1,0}) \approx 0.7892$ and $\lambda_1(\alpha_{1,0}) \approx -0.1360$. Note that the leading-order asymptotic approximation is the predicted pull-in voltage V^* of the standard theory, which was made by Taylor in [22]. A comparison of the one- and two-term asymptotic approximations of V^* is shown in Figure 7 along with the experimental data from [21]. Here, we can see that the two-term asymptotic expansion provides a correction to the predicted pull-in voltage. Also, following the form of equation (4.3), we perform a least squares fit of $V^*(h) = Ah^{3/2} + Bh^{7/2}$ to the experimental data to provide a comparison for our computed coefficients. The results are as follows: $A = 2.09872 \times 10^6$, $B = -2.15799 \times 10^8$ and the coefficient of determination is 0.993478. These values compare

https://doi.org/10.1017/S0956792511000180 Published online by Cambridge University Press

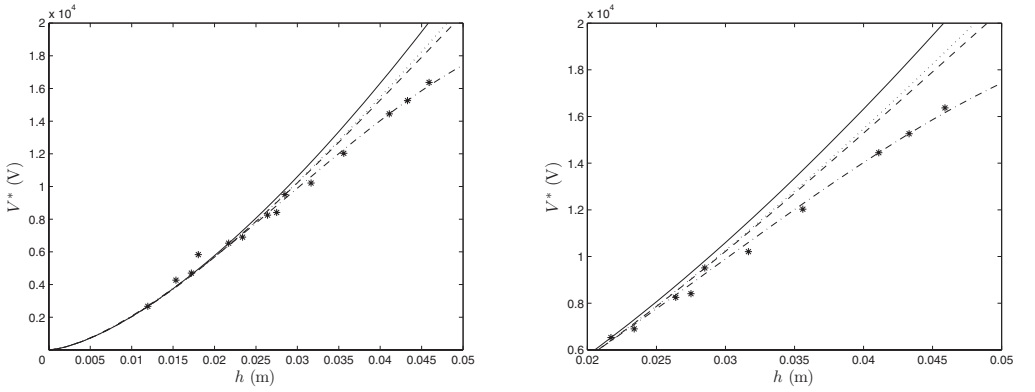


FIGURE 7. (a) Standard theory pull-in voltage (line), two-term asymptotic approximation (dashed), numerical (dotted) and best fit (dashes and dots) versus the plate separation h with the experimental data from [21]. (b) A magnified part of Figure 7(a).

reasonably well with the coefficients of equation (4.3)

$$\sqrt{\lambda_0(\alpha_{1,0})}\sqrt{\frac{2T}{\epsilon_0 L^2}} \approx 2.03993 \times 10^6,$$
$$\frac{\lambda_1(\alpha_{1,0})}{2\sqrt{\lambda_0(\alpha_{1,0})}}\sqrt{\frac{2T}{\epsilon_0 L^6}} \approx -4.89352 \times 10^7.$$

5 Conclusion

We began with the goal of understanding the limitations of the canonical theory of the electrostatically actuated MEMS devices. We identified that because of the small-aspect-ratio approximation, the standard model is really a leading-order asymptotic approximation. In particular, the model neglects the effects of the fringing field and drops small gradient terms. While the former was studied in [15], there was no knowledge about the effect of the latter. Therefore, to understand how this assumption changes the solution set, we constructed a model that retains the small gradient terms. Our system consisted of a simple, idealised elastic membrane held at zero potential suspended above a rigid plate held at potential V. After obtaining the energy of the system – electrostatic and free surface – we used the first variational derivative to develop a new model for the shape of the membrane. Our model captured the Coulomb force in the same way, but included the small gradient terms via the mean curvature operator. We then noted that our theory contained the most important feature of the canonical theory – the existence of a pull-in voltage. This feature is embodied in Theorem 2.2. Next, we focused on our model for the unit disk domain. This allowed for a direct comparison to a well-understood manifestation of the canonical theory. By examining the bifurcation diagram, we found that our model leads to a shift in the pull-in voltage as a function of ϵ. To fully study this behaviour, we found a two-term asymptotic expansion for the first two fold points

https://doi.org/10.1017/S0956792511000180 Published online by Cambridge University Press

– equations (3.18) and (3.19). Next, we compared our predicted pull-in voltage and the canonical approximation to the experimental data of [21]. This comparison showed that our model provided a correction that better approximated the pull-in voltage.

Finally, we conclude with a observation. While this new model provides a correction for the pull-in voltage V^*, Figure 7 shows that for larger h, improvements are still necessary. This would imply, in that region, there are other important forces at work. Moreover, the potential equations are solved only to leading order; consequently, there are some neglected contributions to λ^* at $\mathcal{O}(\epsilon^2)$. The authors are currently considering effects that would correct this problem.

Acknowledgements

The first author (N.D.B.) thanks the National Science Foundation for their support through the Graduate Research Fellowship Program. The second author (J.A.P.) thanks the National Science Foundation (NSF) Award No. 312154. Also, the authors thank Professor John McCuan for his useful discussions concerning the proof of Theorem 2.2. Thanks are also expressed to the referees for numerous useful suggestions.

References

[1] Ackerberg, R. C. (1969) On a nonlinear differential equation of electrohydrodynamics. *Proc. R. Soc. A* **312**(1508), 129–140.

[2] Burns, M. & Grinfeld, M. (2005) Steady state solutions of a bi-stable quasi-linear equation with saturating flux. *Eur. J. Appl. Math.*, Available at CJO, doi:10.1017/S0956792511000076.

[3] Esposito, P., Ghoussoub, N. & Guo, Y. (2010) *Mathematical Analysis of Partial Differential Equations Modeling Electrostatic MEMS*. Courant Lecture Notes. 20, 318. AMS Bookstore.

[4] Feynman, R. P. (1959) There's plenty of room at the bottom. In: *American Physical Society Meeting*, Pasadena, CA, USA. Reprinted in *J. Microelectromech. Syst.* **1**, 60–66.

[5] Finn, R. (1986) *Equilibrium Capillary Surfaces,* Springer-Verlag.

[6] Ghoussoub, N. & Guo, Y. (2007) On the partial differential equations of electrostatic mems devices: Stationary case. *SIAM J. Math. Anal.* **38**(5), 1423–1449.

[7] Gidas, B., Ni, W. M. & Nirenberg, L. (1979) Symmetry and related properties via the maximum principle. *Commun. Math. Phys.* **68**(3), 209–243.

[8] Guo, Y., Pan, Z. & Ward, M. J. (2005) Touchdown and pull-in voltage behavior of a MEMS device with varying dielectric properties. *SIAM J. Math. Anal.* **66** 309–338.

[9] Joseph, D. D. & Lundgren, T. S. (1973) Quasilinear dirichlet problems driven by positive sources. *Arch. Ration. Mech. Anal.* **49**, 241–269, doi:10.1007/BF00250508.

[10] Lindsay, A. E. & Ward, M. J. (2008) Asymptotics of some nonlinear eigenvalue problems for a MEMS capacitor. Part I: Fold point asymptotics. *Methods Appl. Anal.* **15**(3), 297–326.

[11] Lindsay, A. E. & Ward, M. J. (2011) Asymptotics of some nonlinear eigenvalue problems modelling a MEMS Capacitor. Part II: Multiple solutions and singular asymptotics. *Eur. J. Appl. Math.* **22**, 83–123.

[12] Nathanson, H. C., Newell, W. E., Wickstrom, R. A. & Davis, J. R., Jr. (1967) The resonant gate transistor. *IEEE Trans. Electron Devices* **14**(3), 117–133.

[13] Pan, H. (2009) One-dimensional prescribed mean curvature equation with exponential nonlinearity. *Nonlinear Anal. Theory Methods Appl.* **70**(2), 999–1010.

[14] Pelesko, J. A. (2001) Electrostatic field approximations and implications for MEMS devices. In: *Proceedings of ESA*, pp. 126–137.

https://doi.org/10.1017/S0956792511000180 Published online by Cambridge University Press

[15] Pelesko, J. A. (2002) Mathematical modeling of electrostatic MEMS with tailored dielectric properties. *SIAM J. Appl. Math.* **62**(3), 888–908.
[16] Pelesko, J. A. & Bernstein, D. H. (2003) *Modeling MEMS and NEMS*. CRC Press.
[17] Pelesko, J. A., Bernstein, D. H. & McCuan, J. (2003) Symmetry and symmetry breaking in electrostatically actuated MEMS. *Nanotechnology* **2**, 432–435.
[18] Pelesko, J. A. & Chen, X. Y. (2003) Electrostatic deflections of circular elastic membranes. *J. Electrost.* **57**(1), 1–12.
[19] Pelesko, J. A. & Driscoll, T. A. (2005) The effect of the small-aspect-ratio approximation on canonical electrostatic MEMS models. *J. Eng. Math.* **53**(3), 239–252.
[20] Pucci, P. & Serrin, J. (2007) *The Maximum Principle*, Birkhauser.
[21] Siddique, J. I., Deaton, R., Sabo, E. & Pelesko, J. A. (2011) An experimental investigation of the theory of electrostatic deflections. *J. Electrost.* **69**(1), 1–6.
[22] Taylor, G. I. (1968) The coalescence of closely spaced drops when they are at different electric potentials. *Proc. R. Soc. A* **306**(1487), 423–434.

https://doi.org/10.1017/S0956792511000180 Published online by Cambridge University Press